Letters

A Hybrid Control Method to Improve VSC Transient Stability With Considering Current Limit and Power Constraint

Xiaoling Xiong, *Senior Member, IEEE*, Bochen Luo, *Member, IEEE*, Meng Huang, *Member, IEEE*, and Frede Blaabjerg, *Fellow, IEEE*

***Abstract*—Grid-forming (GFM) voltage source converters with current limiting control are prone to losing stability during grid faults. To address this issue, this letter proposes a novel hybrid GFM and grid-following control method combining a specific power design criterion to enhance the transient stability of the system. By adopting appropriate power requirements, the proposed method not only ensures a steady operation of the system after grid faults, but also provides maximum voltage support within the current limit and power constraint. The theoretical analysis is validated by experimental results, which prove the effectiveness of the proposed method.**

***Index Terms*—Current limit, grid-forming (GFM), power constraint, transient stability, voltage support, voltage-source converter (VSC).**

I. Introduction

As THE renewable energy penetration continues to rise, grid-forming (GFM) voltage source converters (VSCs) have gained much attention for their ability to emulate the behavior of traditional synchronous generators (SGs), such as providing voltage and frequency support. Although GFM-VSC can operate as a voltage source such as SG, it still faces significant transient stability challenges during grid faults, especially when the requirements of current limitation, power constraints, and transient grid support are involved [1].

Mode-switching control is the most conventional approach to address the transient stability issues of GFM-VSCs during grid faults, which requires the GFM-VSCs to switch to grid-following (GFL) control mode during grid disturbances, thus conducting power regulation according to the grid code [2]. In this way, the VSC operates like a current source, and its transient stability can be improved by designing appropriate power references. However, the use of phase-locked loops (PLLs) may cause latch-up and wind-up issues, deteriorating system transient performances. Moreover, the transient stability of the system cannot always be guaranteed by pure reactive power injection when severe grid faults occur.

Virtual impedance (VI) or virtual admittance (VA), combining various current limiters, has emerged as a prevalent method to address the transient stability issue during grid faults due to their clear physical significance and simple structure [3]. However, this approach introduces two critical challenges: First, VI/VA will intensify the coupling of active and reactive powers in the system [4]. Besides, the design criteria of VI/VA during static operation and grid faults are different. As a result, the VSC grid support capability is not always maximized [5]. Second, the inserted current limiters will deteriorate the original P-δ curves of the system, causing a reduction of system transient stability margin [6]. Moreover, the fault current is not easy to control when the current limiter saturates, leading to the transient behavior of the VSC being difficult to regulate.

Power reference adjustment is also an effective method to enhance the transient stability of GFM-VSC. By modifying the power references after grid faults, the synchronization of VSC to the grid can be ensured. However, the impact of different power settings on fault current or VSC voltage support capacity has not been fully discussed [3]. Other research also explores some novel control techniques to enhance the VSC transient stability, such as direct current control [4], vector power control [7], and hybrid synchronization control [8]. However, these approaches either compromise the inherent characteristics of SGs or partly rely on the PLL, which limits their use in practice. Besides, the VSC power constraints and maximum grid support during transient events are rarely studied simultaneously.

To address the abovementioned issues, this letter proposes a novel hybrid GFM and GFL control method with specific power design criteria to enhance the transient stability of the system. First, the transient instability mechanism of GFM-VSC with current limiting is revealed. Then, a novel hybrid GFM

Received 29 September 2025; revised 8 November 2025 and 15 December 2025; accepted 2 January 2026. Date of publication 12 January 2026; date of current version 20 March 2026. This work was supported in part by the Smart-Grid National Science and Technology Major Project under Grant 2025ZD0806800 and in part by the National Natural Science Foundation of China under Grant 52277176 and Grant 52222707. *(Corresponding author: Xiaoling Xiong.)*

Xiaoling Xiong and Bochen Luo are with the School of Electrical and Electronic Engineering, North China Electric Power University, Beijing 102206, China (e-mail: xiongxl1102@ncepu.edu.cn; luobochen2024@ncepu.edu.cn).

Meng Huang is with the Hubei Key Laboratory of Power Equipment & System Security for Integrated Energy, School of Electrical Engineering and Automation, Wuhan University, Wuhan 430072, China (e-mail: meng.huang@whu.edu.cn).

Frede Blaabjerg is with the Department of Energy, Aalborg University, DK-9220 Aalborg, Denmark (e-mail: fbl@energy.aau.dk).

Color versions of one or more figures in this article are available at https://doi.org/10.1109/TPEL.2026.3652635.

Digital Object Identifier 10.1109/TPEL.2026.3652635

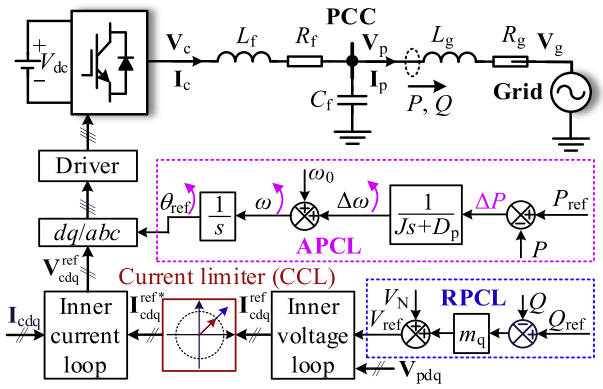

Fig. 1. Topology of the GFM-VSC with current limiting control. APCL: Active power control loop, RPCL: Reactive power control loop.

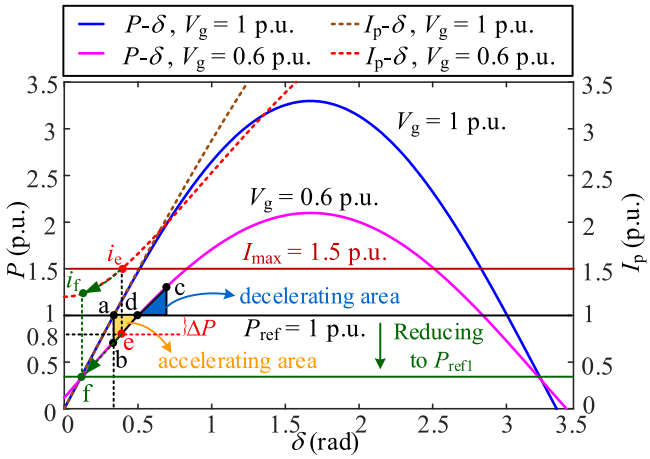

Fig. 2. $P-\delta$ and $I_{\mathrm{p}}-\delta$ curves of the GFM-VSC grid-tied system under normal and grid fault conditions with SCR = 3.

and GFL control method is proposed, and the design criteria for the VSC power references are given, which not only ensure the transient stability of the system after grid faults but can also provide maximum voltage support within current limit and power constraints. Finally, experimental results are presented to verify the effectiveness of the proposed method.

II. Transient Instability Mechanism of GFM-VSC

A. Description of GFM-VSC Grid-Tied System

Fig. 1 shows the topology of a GFM-VSC grid-tied system with a commonly used current limiting method, i.e., adopting a circular current limiter (CCL), where L_{f}, R_{f}, and C_{f} represent the inductance, resistance, and capacitance of the LC filter. R_{g} and L_{g} correspond to the equivalent resistance and inductance of the grid. $\mathbf{V}_{\mathrm{g}} = V_{\mathrm{g}}e^{j\omega_{\mathrm{g}}t}$ and $\mathbf{V}_{\mathrm{p}} = V_{\mathrm{p}}e^{j\theta_{\mathrm{p}}}$ denote the space vectors of grid voltage and point of common coupling (PCC) voltage, $\mathbf{V}_{\mathrm{c}}$, $\mathbf{I}_{\mathrm{c}}$, and $\mathbf{I}_{\mathrm{p}}$ are the space vectors for VSC terminal voltage, terminal current, as well as the PCC current injected to the grid. The above space vectors can also be expressed in the synchronous dq rotating frame. For example, $\mathbf{V}_{\mathrm{p}}$ can be denoted as $\mathbf{V}_{\mathrm{pdq}} = V_{\mathrm{pd}} + \mathrm{j}V_{\mathrm{pq}}$ in the dq frame. Besides, the active and reactive powers injected into the grid are symbolized by P and Q, which are utilized to produce the VSC voltage reference, i.e., $\mathbf{V}_{\mathrm{ref}} = V_{\mathrm{ref}}e^{j\theta_{\mathrm{ref}}}$, through the active power control loop (APCL) and the reactive power control loop (RPCL), respectively. The CCL is inserted between the inner voltage loop and current loop to prevent overcurrent issues, where $\mathbf{I}_{\mathrm{cdq}}^{\mathrm{ref}}$ and $\mathbf{I}_{\mathrm{cdq}}^{\mathrm{ref}^*}$ are the current references before and after the current limiter.

B. Transient Instability Mechanism With Current Limiter

According to the topology of the GFM-VSC grid-tied system shown in Fig. 1, the active and reactive power injected into the grid can be derived as follows:

$$P = \frac{3}{2}V_{\mathbf{p}}I_{\mathbf{pd}} = \frac{3}{2}V_{\mathbf{p}}\frac{(V_{\mathbf{p}} - V_{\mathbf{g}}\cos\delta)\,R_{\mathbf{g}} + X_{\mathbf{g}}V_{\mathbf{g}}\sin\delta}{R_{\mathbf{g}}^2 + X_{\mathbf{g}}^2} \quad (1)$$

$$Q = -\frac{3}{2}V_{\mathbf{p}}I_{\mathbf{pq}} = \frac{3}{2}V_{\mathbf{p}}\frac{(V_{\mathbf{p}} - V_{\mathbf{g}}\cos\delta)\,X_{\mathbf{g}} - R_{\mathbf{g}}V_{\mathbf{g}}\sin\delta}{R_{\mathbf{g}}^2 + X_{\mathbf{g}}^2} \quad (2)$$

TABLE I
Parameters of the VSC Grid-Tied System

Symbol	Parameter	Value
V_{g}	Peak value of rated voltage	1 p.u. (70 V)
S_{N}	Rated power	1 p.u. (1 kVA)
f_{N}	Fundamental frequency	1 p.u. (50 Hz)
SCR	Short-circuit ratio	3
L_{f}	Inductance of LC filter	0.167 p.u.
C_{f}	Capacitance of LC filter	0.0354 p.u.
f_{s}	Sampling frequency	10 kHz
r	R/X ratio	0.2
J	Virtual inertia	5 p.u.
D_{p}	Damping coefficient	40 p.u.
m_{q}	Q-V droop gain	0.1 p.u.
k_{pI}	Proportional gain of current loop	0.98
k_{iI}	Integral gain of current loop	3.51
k_{pP}	Proportional gain of outer P loop	0.0024
k_{pQ}	Proportional gain of outer Q loop	0.0024
k_{iQ}	Integral gain of outer Q loop	0.476

where δ is the power angle, which is defined as the phase difference between $\mathbf{V}_{\mathrm{p}}$ and $\mathbf{V}_{\mathrm{g}}$, i.e., $\delta = \theta_{\mathrm{ref}} - \omega_{\mathrm{g}}t$. I_{pd} and I_{pq} are the dq components of $\mathbf{I}_{\mathrm{p}}$. Based on them, the amplitude of $\mathbf{I}_{\mathrm{p}}$ can also be calculated, being expressed as follows:

$$I_{\mathbf{p}} = \sqrt{I_{\mathbf{pd}}^2 + I_{\mathbf{pq}}^2} = \sqrt{\frac{{V_{\mathbf{p}}}^2 - 2V_{\mathbf{p}}V_{\mathbf{g}}cos\delta + {V_{\mathbf{g}}}^2}{R_{\mathbf{g}}^2 + X_{\mathbf{g}}^2}}. \quad (3)$$

Further, considering the control effect of RPCL and taking it into (2), the relationships of V_{p} and δ, i.e., V_{p} (δ), can be deduced as (4), shown at the bottom of this next page. Then, substituting V_{p} (δ) into (1) and (3), the $P-\delta$ and $I_{\mathrm{p}}-\delta$ curves under different grid conditions can be plotted, as shown in Fig. 2, where the detailed parameters of the system are presented in Table I in Section IV. The design of J, D_{p}, m_{q}, follows the standard 20242962-T-524 "Technical specification for grid-forming converter" in China. From Fig. 2, it can be seen that the VSC can stabilize at the rated operation point "a" under

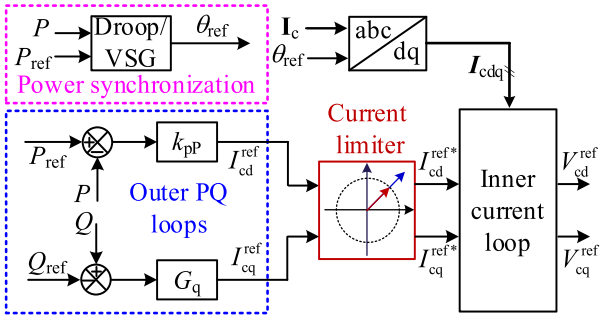

Fig. 3. Structure of the novel hybrid control method for the VSC.

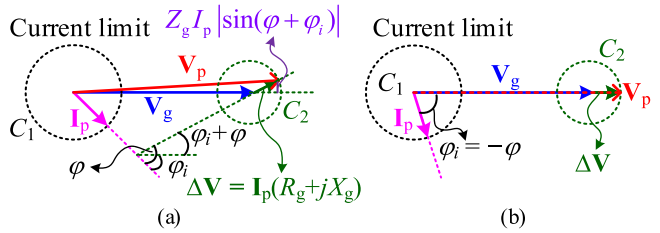

Fig. 4. Phasor diagram of the VSC grid-tied system. (a) $\varphi_i \neq -\varphi$. (b) $\varphi_i = -\varphi$.

normal grid conditions with $P = 1$ p.u., where $I_{\rm p}$ is also about 1 p.u., indicating that the VSC does not have overcurrent risk and instability issues. When a 40% voltage sag occurs, the operation point of the system will jump from "a" to "b", and δ is going to increase because of the accelerating area. After the operation point reaches the upper bound "c", δ is about to decrease and will finally stabilize at the new equilibrium point "d" due to the decelerating area based on the equal area criterion [6]. However, if the current limit of VSC is further considered, such as $I_{\rm max} = 1.5$ p.u., as shown in Fig. 2, the output current will be limited at $i_{\rm e}$, and δ will be restricted at "e" accordingly. Since P is smaller than the reference, i.e., $P_{\rm ref} = 1$ p.u., a control error ΔP can not be eliminated, finally resulting in transient instability, as shown in Fig. 1.

III. Transient Stability Enhanced Method

A. Proposed Hybrid GFM and GFL Control Method

The above results indicate that the saturated current limiter will cause the reduction of output power during grid faults, and the mismatch between P and $P_{\rm ref}$ is the main reason for transient instability. Hence, it is necessary to decrease the active power reference after grid faults to restabilize the system. As shown in Fig. 2, when $P_{\rm ref}$ is reduced to a new given value $P_{\rm ref1}$, the operation point will move from "e" to "f" after voltage dips, and $I_{\rm p}$ will shift from "$i_{\rm e}$" toward "$i_{\rm f}$" accordingly, which not only ensures the existence of a steady-state operating point after the grid fault but also reduces the overcurrent risk. Moreover, due to the power coupling effect, the output reactive power of traditional GFM-VSC is not easy to regulate quantitatively, so the power constraint of VSC is always overlooked.

To address these issues, a novel hybrid GFM and GFL control method is proposed in this letter, as shown in Fig. 3. The synchronous control loop based on power is still used to synchronize with the grid, but the power control loops adopt GFL structures, such as outer PQ control loops. To prevent the conflict of power regulation in APCL and the outer P control loop, the APCL only uses a proportional controller to maintain the *P-f* droop behavior. $G_{\rm q} = k_{\rm pQ} + k_{\rm iQ}/s$ is the transfer function of the outer reactive power controller. Moreover, the CCL can also be inserted to prevent transient current overshoot. To this end, the VSC with the proposed hybrid control method can adjust its output power flexibly during grid faults like GFL-VSCs but without PLL issues, and the power coupling effect can also be alleviated. Thereby, the transient stability of the system can be enhanced by power regulation within the current limit and power constraint. Meanwhile, the voltage support capacity of the VSC can also be maximized by designing appropriate power references, which will be presented in the next section.

B. VSC Power Design Criteria During Grid Faults

According to Fig. 1, the steady-state operation equation of the system from PCC to the grid can be described as follows:

$$\begin{aligned} V_{\mathbf{pd0}} &= V_{\mathbf{gd0}} + R_{\mathbf{g}} I_{\mathbf{pd0}} - X_{\mathbf{g}} I_{\mathbf{pq0}} \\ V_{\mathbf{pq0}} &= V_{\mathbf{gq0}} + R_{\mathbf{g}} I_{\mathbf{pq0}} + X_{\mathbf{g}} I_{\mathbf{pd0}} \\ V_{\mathbf{gd0}}^2 &+ V_{\mathbf{gq0}}^2 = V_{\mathbf{g}}^{\mathbf{2}} \end{aligned} \tag{5}$$

where the subscript "0" means the steady-state value.

As $\mathbf{V}_{\rm p}$ is aligned with the d-axis, i.e., $V_{\rm pq0} = 0$, the d-axis component of $\mathbf{V}_{\rm g}$ can be deduced as follows:

$$V_{gd0} = \sqrt{V_g^2 - (R_g I_{pq0} + X_g I_{pd0})^2}. \tag{6}$$

If (6) has a solution, the following expression should be satisfied:

$$V_{\mathbf{g}} \geq |R_{\mathbf{g}} I_{\mathbf{pq0}} + X_{\mathbf{g}} I_{\mathbf{pd0}}| = Z_{\mathbf{g}} I_{\rm p} \, |\cos\varphi \sin\varphi_{\mathbf{i}} + \sin\varphi \cos\varphi_{\mathbf{i}}| \tag{7}$$

where φ , $\varphi_{\rm i}$ are the grid impedance angle and output current phase angle, respectively. $Z_{\rm g}$ is the amplitude of grid impedance.

When $\varphi_{\rm i} = -\varphi$, the inequality in (7) can be simplified as follows:

$$V_g \geq Z_g I_p \, |\sin(\varphi + \varphi_i)| = 0. \tag{8}$$

From (8), it can be seen that if $\mathbf{I}_{\rm p}$ lags $\mathbf{V}_{\rm p}$ by an angle of φ, the steady-state solutions of the system will always exist as long as $V_{\rm g} \geq 0$, even in the worst case of $V_{\rm g} = 0$.

Fig. 4 further gives the phasor diagram of the VSC grid-tied system under different operating conditions. As shown in Fig. 4(a), $\mathbf{I}_{\rm p}$ is limited in C_1 due to the effect of the current

$$V_p = \frac{1.5 m_q X_g V_g \cos\delta - \left(R_g{}^2 + X_g{}^2\right) + \sqrt{\left(R_g{}^2 + X_g{}^2 - 1.5 m_q X_g V_g \cos\delta\right)^2 + 6 m_q{}^2 X_g R_g V_g \sin\delta + 6 m_q{}^2 X_g \left(R_g{}^2 + X_g{}^2\right) Q_{ref} + 6 m_q X_g \left(R_g{}^2 + X_g{}^2\right) V_N}}{3 m_q X_g}. \tag{4}$$

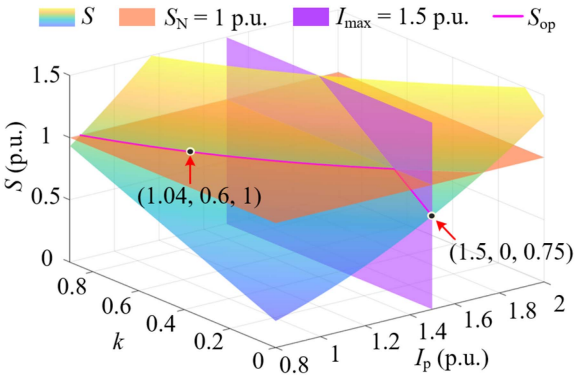

Fig. 5. 3-D plot of S under different operation conditions and its optimally designed values considering $S_N = 1\ p.u.$ and $I_{\max} = 1.5 p.u.$.

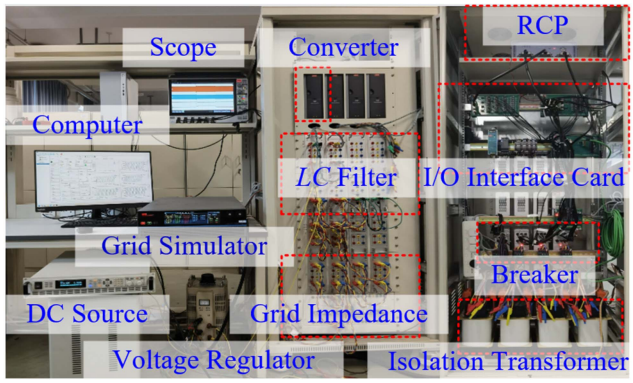

Fig. 6. Experimental platform of the grid-tied VSC.

limiter, which will force $\Delta\mathbf{V}$ to move in C_2 and cause the terminal point of $\mathbf{V}_\mathrm{p}$ to be located in C_2 too. However, due to $\varphi_\mathrm{i} \neq -\varphi$, the direction of $\mathbf{V}_\mathrm{p}$ is not the same as $\mathbf{V}_\mathrm{g}$, thus V_p can not be maximized. Fortunately, if φ_i is equal to $-\varphi$, as shown in Fig. 4(b), $\mathbf{V}_\mathrm{p}$ will be as large as $\mathbf{V}_\mathrm{g}$ plus $\Delta\mathbf{V}$, i.e., $V_\mathrm{p} = V_\mathrm{g} + \Delta V$, representing the best voltage support capability. The above analysis indicates that when $\varphi_\mathrm{i} = -\varphi$, the VSC not only can withstand the worst grid fault, i.e., $V_\mathrm{g} = 0$, but also provides maximum voltage support during the grid fault. This conclusion is almost aligned with the findings mentioned in [3], where it is reported that the transient stability will be enhanced when the saturation current phase angle φ_i increases. However, the fundamental mechanism for this phenomenon has not been clarified, and how to realize the optimal operation for VSC during grid faults has not been discussed either. To extend previous works, this letter tries to address these issues through flexible transient power control by using the proposed hybrid control method. In such a case, the dq component of the PCC output current can be written as follows:

$$\begin{cases} I_{pd0} = I_p \cos\varphi \\ I_{\mathrm{pq0}} = -I_p \sin\varphi. \end{cases} \tag{9}$$

Accordingly, the output active and reactive powers at PCC can also be calculated, as follows:

$$\begin{cases} P = \left(k\frac{I_\mathrm{p}}{I_\mathrm{N}} + \frac{1}{\mathrm{SCR}}\left(\frac{I_\mathrm{p}}{I_\mathrm{N}}\right)^2\right) S_\mathrm{N} \cdot \cos\varphi = S \cdot \cos\varphi \\ Q = \left(k\frac{I_\mathrm{p}}{I_\mathrm{N}} + \frac{1}{\mathrm{SCR}}\left(\frac{I_\mathrm{p}}{I_\mathrm{N}}\right)^2\right) S_\mathrm{N} \cdot \sin\varphi = S \cdot \sin\varphi \end{cases} \tag{10}$$

where S_N and I_N are the rated power and rated current of the VSC, while S is the VSC operating capacity. k is a factor denoting different voltage dips. For example, when a 40% voltage sag occurs, k should be taken as 0.6. Based on (10), the 3-D view of S under different voltage sags and current output conditions can be plotted, as shown in Fig. 5. If the power constraint and current limit are further considered, such as $S_\mathrm{N} = 1$ p.u. and $I_{\max} = 1.5$ p.u., shown as the orange and purple surfaces, the optimal values for S can be obtained at the intersections of S, S_N, and $I_{\max}$, which can be expressed as follows:

$$S_{op} = \begin{cases} S_N, & \left(\frac{I_N}{I_{\max}} - \frac{I_{\max}/I_N}{SCR}\right) \leq k \leq 0.9 \\ \left(\frac{kI_{\max}}{I_N} + \frac{\left(I_{\max}/I_N\right)^2}{SCR}\right) S_N, & 0 \leq k \leq \left(\frac{I_N}{I_{\max}} - \frac{I_{\max}}{I_N SCR}\right) \end{cases} \tag{11}$$

From the S_op shown in Fig. 5, when V_g drops to 0 p.u. (corresponding to the most severe grid fault), S should decrease to about 0.75 p.u., thus ensuring transient stability and current limiting requirements. Meanwhile, when a 40% voltage sag occurs, i.e., $V_\mathrm{g} = 0.6$ p.u., S needs to be 1 p.u. because of the power constraint, which will restrict I_p at about 1.04 p.u., within the current limiting requirement. It is worth noting that the implementation of the above optimal power design criteria requires the grid-side information, such as the SCR and grid impedance angle φ. Although they can be obtained by the online impedance estimation method proposed in [9], [10], [11], it will increase the complexity of practical application. To address this issue, the power design criteria given in (11) can be optimized based on the PCC voltage, thus reducing its reliance on grid information, which can be deduced as follows:

$$S_{op} = \begin{cases} S_N, & \frac{I_N V_N}{I_{\max}} \leq V_p \leq 0.9 V_N \\ 1.5 V_p I_{\max}, & 0 \leq V_p \leq \frac{I_N V_N}{I_{\max}}. \end{cases} \tag{12}$$

In this way, these designed power values not only can give rapid and maximized voltage support during transient processes, but also be easier to implement in practice. In contrast, this power design criterion may not be easily applicable to conventional GFM-VSCs employing Q-V droop control, as the power coupling effect will hinder the independent regulation of active and reactive powers.

IV. Experimental Verification

To verify the correctness of the theoretical analysis and effectiveness of the proposed method, an experimental platform of a grid-tied VSC is built in the laboratory, as shown in Fig. 6. The parameters of the system are listed in Table I. To prevent the current overshoot during the VSC startup and grid connection process, a presynchronization with the PLL is adopted to match

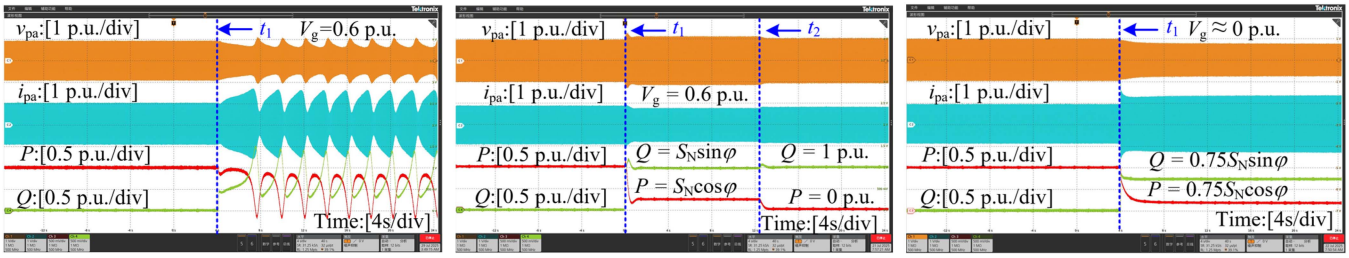

Fig. 7. Measured waveforms of the VSC adopting different control methods under grid faults. (a) Traditional GFM control method with CCL under 40% voltage sag. (b) Proposed method with optimal power design under 40% voltage sag. (c) Proposed method with optimal power design under about 100% voltage sag.

the voltage amplitude, phase, and frequency before closing the breaker.

Fig. 7(a) shows the experimental waveforms of the VSC using the traditional GFM method with current limiting. The VSC first stabilizes at the rated operation point before $t = t_1$. Then, a 40% voltage sag happens at t_1, it can be seen that due to the effect of CCL, the output current is limited and the active power cannot be adjusted to the given value, i.e., $P_{\text{ref}} = 1$ p.u. Hence, the system loses its stability after t_1, which is consistent with the theoretical analysis in Fig. 2. Fig. 7(b) further gives the experimental waveforms using the proposed hybrid control method.

In contrast to the experimental results in Fig. 7(a), the VSC can synchronize with the grid using the optimally designed power values mentioned in Fig. 5 when a 40% voltage sag occurs at $t = t_1$. Meanwhile, the voltage support effect is better than the pure reactive power injection method after t_2. Moreover, the effectiveness of the proposed method under the most severe fault, i.e., $V_g \approx 0$, is also tested by experiment, as shown in Fig. 7(c), where V_g jumps from 1 p.u. to about 0 p.u. at t_1. It can be seen that the system still works stably when the optimally designed value, i.e., $S = 0.75$ p.u., is adopted, which ensures the fault current to be lower than $I_{\max} = 1.5$ p.u. The above experimental results agree well with the theoretical analysis mentioned in Figs. 4 and 5, indicating the proposed control method with optimal power design not only improves the transient stability of the system but also provides maximum voltage support under the current limit and power constraint.

V. Conclusion

In this letter, the transient instability mechanism of the GFM-VSCs with current limiting control is investigated. It is found that the mismatch between P and P_{ref} caused by the limited current is the main reason for transient instability. Thus, a novel hybrid GFM and GFL control method with appropriate power design criteria is presented, which not only enhances the transient stability of the system but can also provide maximum voltage support under current limit and power constraint. The effectiveness of the proposed method is verified by experiments.

References

[1] M. G. Taul, X. Wang, P. Davari, and F. Blaabjerg, "An overview of assessment methods for synchronization stability of grid-connected converters under severe symmetrical grid faults," *IEEE Trans. Power Electron.*, vol. 34, no. 10, pp. 9655–9670, Oct. 2019.

[2] X. Xiong, C. Wu, and F. Blaabjerg, "An improved synchronization stability method of virtual synchronous generators based on frequency feedforward on reactive power control loop," *IEEE Trans. Power Electron.*, vol. 36, no. 8, pp. 9136–9148, Aug. 2021.

[3] N. Baeckeland, D. Chatterjee, M. Lu, B. Johnson, and G.-S. Seo, "Overcurrent limiting in grid-forming inverters: A comprehensive review and discussion," *IEEE Trans. Power Electron.*, vol. 39, no. 11, pp. 14493–14517, Nov. 2024.

[4] Z. Zeng, D. Yang, H. Wu, L. Shu, Y. Sun, and S. Wang, "A direct current-synchronization control for voltage source converter with enhanced fault ride-through capability," *IEEE Open J. Power Electron.*, vol. 5, pp. 1484–1499, 2024.

[5] H. Wu, X. Wang, and L. Zhao, "Design considerations of current-limiting control for grid-forming capability enhancement of VSCs under large grid disturbances," *IEEE Trans. Power Electron.*, vol. 39, no. 10, pp. 12081–12085, Oct. 2024.

[6] B. Fan and X. Wang, "Equivalent circuit model of grid-forming converters with circular current limiter for transient stability analysis," *IEEE Trans. Power Syst.*, vol. 37, no. 4, pp. 3141–3144, Jul. 2022.

[7] K. Ji, H. Lu, and M. Wang, "A vector-power synchronization control for grid-forming voltage-source converters with enhanced performance under wide SCR condition," *IEEE Trans. Power Del.*, vol. 39, no. 4, pp. 2507–2519, Aug. 2024.

[8] L. Harnefors, J. Kukkola, M. Routimo, M. Hinkkanen, and X. Wang, "A universal controller for grid-connected voltage-source converters," *IEEE J. Emerg. Sel. Top. Power Electron.*, vol. 9, no. 5, pp. 5761–5770, Oct. 2021.

[9] J. Fang, H. Deng, and S. M. Goetz, "Grid impedance estimation through grid-forming power converters," *IEEE Trans. Power Electron.*, vol. 36, no. 2, pp. 2094–2104, Feb. 2021.

[10] J. Sun, J. Yu, J. Qiu, and Y. Wang, "Transient-responses-based grid impedance estimation for grid-forming converters," in *Proc. 4th Int. Conf. Elect. Eng. Control Technol.*, 2022, pp. 741–745.

[11] R. E. Betz and M. G. Taul, "Identification of grid impedance during severe faults," in *Proc. IEEE Energy Convers. Congr. Expo.*, 2019, pp. 1076–1082.